EARTH SURFACE PROCESSES AND LANDFORMS
Earth Surf. Process. Landforms (2018)

Published online in Wiley Online Library
(wileyonlinelibrary.com) DOI: 10.1002/esp.4353

Landslides control the spatial and temporal variation of channel width in southern Taiwan: Implications for landscape evolution and cascading hazards in steep, tectonically active landscapes

Brian J. Yanites,[1]* Nate A. Mitchell,[1] Joshua C. Bregy,[2] Grace A. Carlson,[1] Kirstyn Cataldo,[1] Margaret Holahan,[1] Graham H. Johnston,[1] Amelia Nelson,[1] Jeffery Valenza[1] and Matthew Wanker[1]
[1] Department of Earth and Atmospheric Sciences, Indiana University, Bloomington, IN
[2] Department of Geography, Indiana University, Bloomington, IN

Received 24 August 2017; Revised 13 January 2018; Accepted 18 January 2018

*Correspondence to: Brian J. Yanites, Department of Earth and Atmospheric Sciences, Indiana University, Bloomington, IN, USA. E-mail: byanites@indiana.edu

ESPL
Earth Surface Processes and Landforms

ABSTRACT: Intense precipitation or seismic events can generate clustered mass movement processes across a landscape. These rare events have significant impacts on the landscape, however, the rarity of such events leads to uncertainty in how they impact the entire geomorphic system over a range of timescales. Taiwan is steep, tectonically active, and prone to landslide and debris flows, especially when exposed to heavy rainfall events. Typhoon Morakot made landfall in Taiwan in August of 2009, causing widespread landslides in southern Taiwan. The south to north trend in valley relief in southern Taiwan leads to spatial variability in landslide susceptibility providing an opportunity to infer the long-term impact of such landslide events on channel morphology. We use pre- and post-typhoon imagery to quantify the propagating impact of this event on channel width as the debris is routed through the landscape. The results show the importance of cascading hazards from landslides on landscape evolution based on patterns of channel width (both pre- and post-typhoon) and hillslope gradients in 20 basins along strike in southern Taiwan. Prior to Typhoon Morakot, the river channels in the central part of the study area were about 3–10 times wider than the channels in the south. Following the typhoon, aggradation and widening was also a maximum in these central to northern basins where hillslope gradients and channel steepness is high, accentuating the pre-typhoon pattern. The results further show that the narrowest channels are located where channel steepness is the lowest, an observation inconsistent with a detachment-limited model for river evolution. We infer this pattern is indicative of a strong role of sediment supply, and associated landslide events, on long-term channel evolution. These findings have implications across a range of spatial and temporal scales including understanding the cascade of hazards in steep landscapes and geomorphic interpretation of channel morphology. Copyright © 2018 John Wiley & Sons, Ltd.

KEYWORDS: landslides; fluvial geomorphology; channel width; tectonic geomorphology; hazards

Introduction

The topography of steep landscapes is a product of the geomorphic processes that erode and transport material over a range of spatial and temporal scales. In tectonically active regions, most geomorphic work is accomplished during discrete atmospheric and seismic events. These occur as either frequent, low-magnitude events that gradually shape landscapes (Wolman and Miller, 1960), such as annual floods resulting from seasonal precipitation patterns, or as rare, high-magnitude events, such as intense storms and earthquakes, that dramatically alter a landscape in a short period of time (Yanites *et al.*, 2010a; Parker *et al.*, 2011; Anderson *et al.*, 2015; Rathburn *et al.*, 2017). The effects of rare events on landscape evolution, however, are poorly constrained due to limited observational data. Moreover, these rare, high-impact events are often hazards to the communities living on and near landforms experiencing the most change (e.g. Chen and Petley, 2005). It is therefore imperative to quantify landscape responses to such events in order to better mitigate these hazards as well as understand the importance of these rare events in landscape evolution.

An example of a recent high-magnitude event is Typhoon Morakot, which made landfall in Taiwan on August 7, 2009 and delivered extreme rainfall to the southern portion of the island (Chien and Kuo, 2011). Studies have documented that > 22 000 landslides occurred as a result of this typhoon, which is comparable to recent seismically driven events (Lin *et al.*, 2011; Huang *et al.*, 2017). The massive amount of sediment mobilized by this event is now propagating through local fluvial systems. This causes a cascade of significant geomorphic

change and hazards where the impacts of the event continue to propagate through a system, threatening life and property. Our objective is to document downstream impacts of these landslides to improve quantitative constraints on landscape response to rare, high-magnitude events and to place the results into the context of how such events shape the landscape. We perform this analysis along a steep topographic gradient resulting from the tectonic setting of Taiwan (Figure 1). This topographic pattern sets up a gradient in landslide susceptibility and provides an opportunity to explore the long-term impact of such events on the geomorphology of the fluvial systems draining the landscape. The results have implications for both hazard mitigation strategies as well as understanding controls on channel morphology in steep, highly erosive environments. Furthermore, a deeper understanding of the potential downstream effects related to large scale landslide events and the related impacts on population centers may also improve our predictive abilities for the propagation of hazards by future landslide events (Robinson and Davies, 2013; Dingle *et al.*, 2017), thereby reducing the losses associated with such

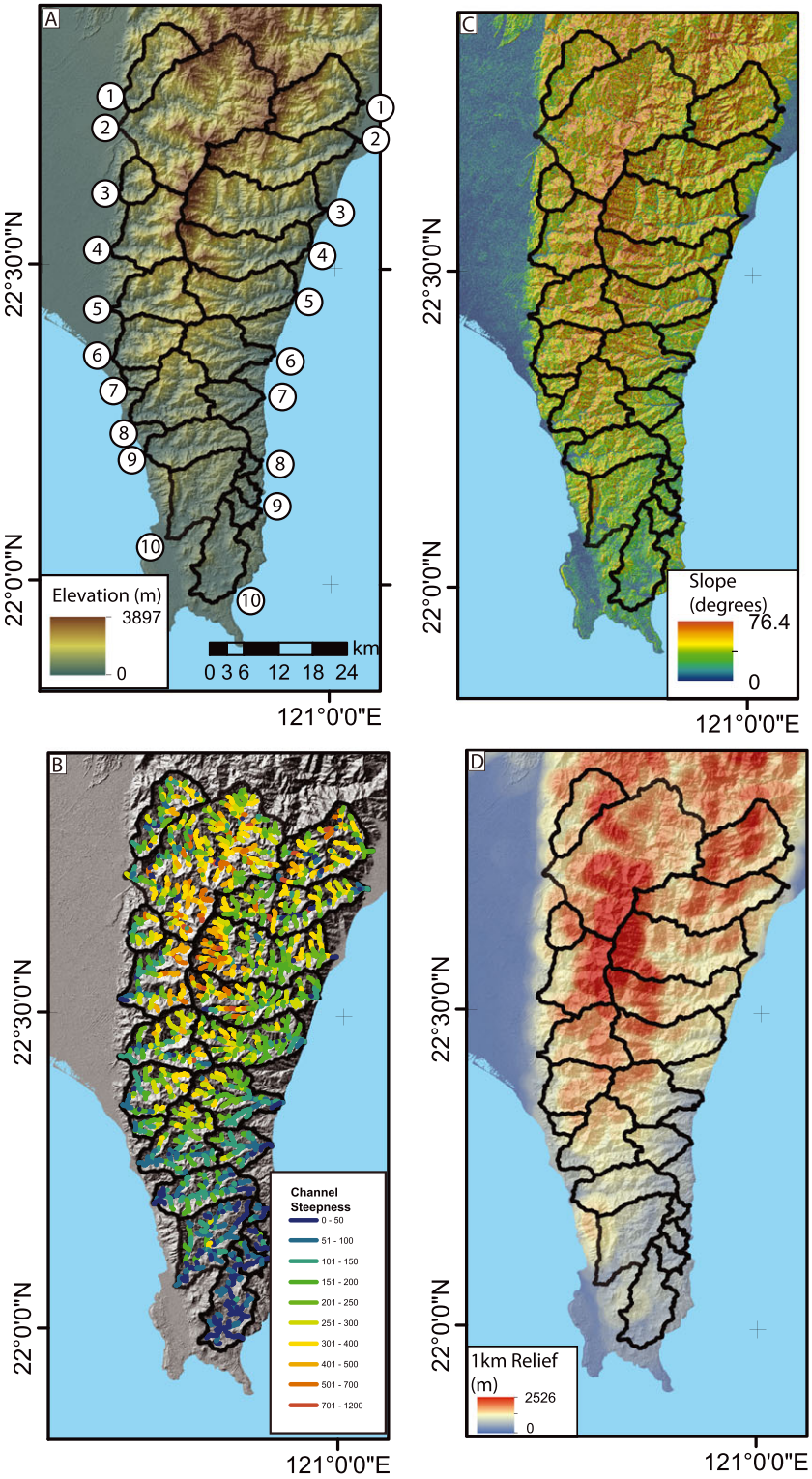

Figure 1. Topography and geomorphic metrics of the study area in southern Taiwan. (A) Elevation and watershed numbers are indicated; (B) channel steepness averaged over 1 km reaches in each basin; (C) pattern of hillslope gradients; (D) distribution of relief over 1 km circular windows. [Colour figure can be viewed at wileyonlinelibrary.com]

catastrophic geomorphic events. Insights gained from observing landscape response to individual events provide important context for understanding how rare or extreme events influence landscape evolution.

Previous work has shown that the effects of regional mass wasting events due to earthquakes or extreme precipitation have the ability to produce significant change across the landscape (Goswami, 1985; Pearce and Watson, 1986; Anderson *et al.*, 2015; Rathburn *et al.*, 2017) with the potential for generating a lasting imprint on the landscape (Yanites *et al.*, 2011). For example, the 1929 M_w 7.3 Murchison earthquake in New Zealand resulted in a massive influx of sediment to river channels (~4×10^5 m^3 km^{-2}) that persisted for at least 50 years (Pearce and Watson, 1986), indicating that earthquake-induced landslides act as an important sediment delivery mechanism that can impact the river system for decades. Following the Assam earthquake in 1950, significant river aggradation occurred immediately following the seismic event (Poddar, 1952) which continued to influence downstream river dynamics along the Brahmaputra until at least the late 1970s (Goswami, 1985). In Taiwan, the damaging 1999 M_w 7.6 Chi-Chi earthquake and subsequent typhoons induced over 50 000 landslides across central Taiwan (Hung, 2000; Dadson *et al.*, 2004). These landslides had significant downstream impacts including increased fluvial suspended sediment discharge in the following few years after the event (Dadson *et al.*, 2004; Hovius *et al.*, 2011) and significant aggradation (3–12 m) of river beds due to excess bedload that persisted for at least a decade (Hsu *et al.*, 2010) and may persist for up to a century following the earthquake (Yanites *et al.*, 2010a). The 2008 M_w 7.9 Wenchuan earthquake caused extensive landslides that led to significant changes in sediment dynamics in the regional rivers (Wang *et al.*, 2015; Li *et al.*, 2016). Recently, the 2015 Gorkha, Nepal earthquake (M_w 7.8) caused extensive avalanches and landslides (Kargel *et al.*, 2016; Roback *et al.*, 2018) which may impact river processes in the future as the material is mobilized during the monsoon season.

Recent work has recognized the importance of understanding cascading effects of natural disasters to fully mitigate the hazards of such events (Nguyen *et al.*, 2013; Budimir *et al.*, 2014). Landslides, especially when regionally clustered due to events such as earthquakes or extreme precipitation, are one example of a cascading hazard. While the landslides themselves can be quite catastrophic (Tsou *et al.*, 2011), the propagating impacts of the landslide material through the landscape can cause significant, long-lived hazards (Nguyen *et al.*, 2013). For example, aggradation in downstream riverbeds following the event can change flood inundation patterns and frequency (Stover and Montgomery, 2001; Chen and Petley, 2005; Lane *et al.*, 2007; Robinson and Davies, 2013; Croissant *et al.*, 2017a) as well as influence channel bank mobility (Lisle, 1982; Lane *et al.*, 2007). Regions with mountainous topography and high populations, such as Taiwan, are particularly vulnerable to cascading hazards associated with regional landsliding initiated by earthquakes and extreme precipitation. Although the recognition that such events can impact river processes for decades has been documented (e.g. Goswami, 1985; Pearce and Watson, 1986; Yanites *et al.*, 2010a), relatively little work has focused on documenting the downstream impacts of regional landslide events on fluvial morphology immediately following the event.

Over longer timescales, the cumulative impact of sediment supply events from hillslopes can potentially have a significant impact on the morphodynamics of downstream river channels (Sklar and Dietrich, 2006; Yanites *et al.*, 2011; Dingle *et al.*, 2017). Sediment can provide the tools for active erosion processes on the bottom of a river channel but can also inhibit erosion processed by blanketing the bedrock in a thick alluvial cover. Large, regional events such as Typhoon Morakot drive aggradation and arrest fluvial incision processes from occurring while the sediment is being evacuated. Such sediment impulse events thus act to lower erosional efficiency processes, potentially leading to long-term channel steepening. The timescale of response compared to the frequency of pulses of sediment input is therefore an important consideration to determine if such events have a long-term impact on landform morphology and landscape evolution. Documenting the spatial and temporal response to sediment impulse events, and comparing with pre-event morphology, will provide key insights into determining the importance of these events on the topography of the region.

Our focus here is to quantify channel width along strike in southern Taiwan (Figure 1). The purpose of this is two-fold: (1) characterize the pattern of channel width along a spatial gradient in topography and (2) document the initial fluvial response to intense landslide activity associated with Typhoon Morakot as a starting point for understanding the cascading impacts of regional landslide events through the landscape. This is accomplished by analyzing pre- and post-typhoon satellite imagery for major drainage basins throughout the study area. A detailed analysis of the spatiotemporal patterns of channel width, drainage basin area, hillslope morphology, and channel steepness will advance our understanding of the geomorphic processes and cascading hazards that arise from extreme weather events. Additionally, observations from this rare, high-magnitude event will provide insight on the long-term dynamics of river systems in southern Taiwan.

Field Area

Topographic setting

The Hengchung peninsula in southern Taiwan is the product of the oblique collision between the Philippine Sea Plate and the eastern margin of Eurasia (Suppe, 1984; Wiltschko *et al.*, 2010). The topography rises from maximum elevations of only a few hundred meters in the south to almost 4 km in the north (Figure 1a). The topography along this gradient is underlain primarily by a low-grade slate (Wiltschko *et al.*, 2010) and shows a clear gradient of increasing slope and relief from the south to north (Figure 1). Furthermore, thermochronology data are unreset in the south and reset in the north, suggesting a north–south (N–S) gradient in total exhumation (Fuller *et al.*, 2006; Hsu *et al.*, 2016). Cosmogenic beryllium-10 (^{10}Be) concentrations in quartz river sands show a gradual increase of hillslope erosion rates from south to north as well (Derrieux *et al.*, 2014; Chen *et al.*, 2015). Using the natural experiment set up by the topographic gradient and relatively uniform rock type, we explore the magnitude of geomorphic processes in response to an extreme precipitation event and place the results in context with long-term landscape evolution of the region.

Typhoon Morakot

Typhoon Morakot made landfall in Taiwan on August 7, 2009, and slowly moved across the island before entering the Taiwan Strait 24 hours later (Figure 2). While only reaching Category 1 status on the Saffir–Simpson hurricane wind scale (V_{max} = 41 m s^{-1} for Morakot), the storm produced substantial volumes of precipitation (Hendricks *et al.*, 2015). Rain gauges in the mountains recorded 24 hours of accumulated rainfall exceeding 500 mm (maximum: 800 mm) and 700 mm (maximum:

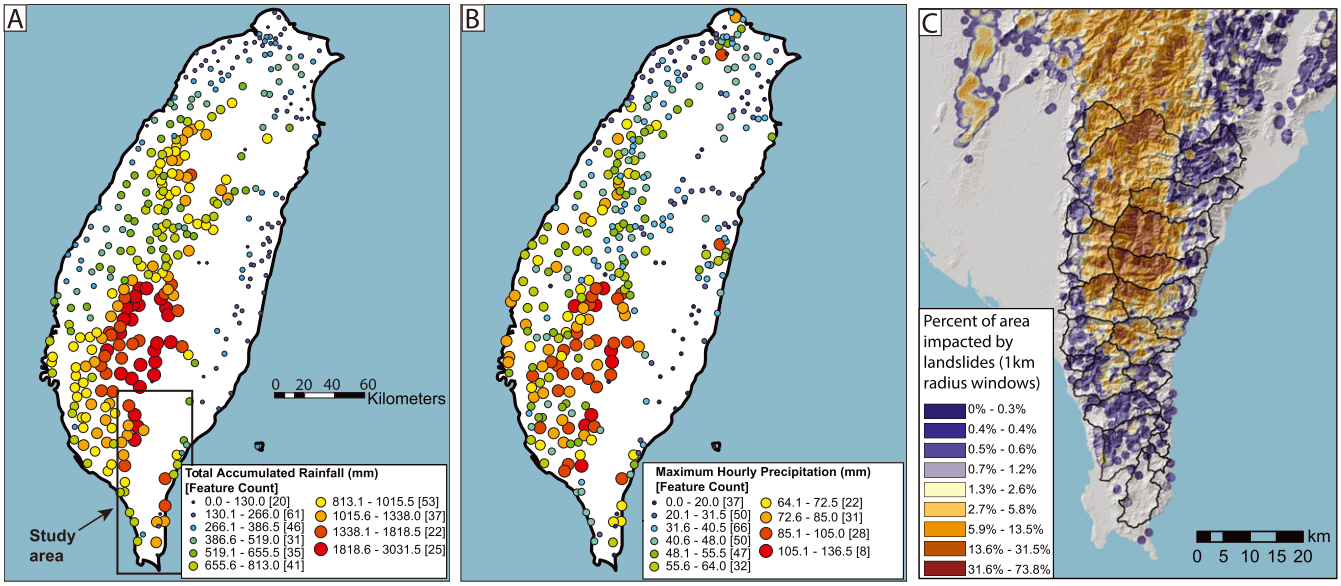

Figure 2. Patterns of precipitation associated with Typhoon Morakot from rain gauge data. (A) Total accumulated rainfall between August 4 and 12, 2009. Note this includes the days leading up to the actual landfall. (B) Maximum precipitation intensity over one hour period. Note that rain gauges are absent in many high mountain regions, where a notable orographic effect likely enhanced rainfall even more. (C) Distribution of landslides in August of 2009 (Lin *et al.*, 2011; Huang *et al.*, 2017). The image is generated from a spatial coverage of disturbed land observed with the FORMOSAT-2 satellite. Each pixel is colored by the percent of area within a 1 km radius of that pixel that experienced landsliding during Typhoon Morakot. [Colour figure can be viewed at wileyonlinelibrary.com]

> 1200 mm) on August 7 and 8, respectively (Chien and Kuo, 2011) (Figure 2). In total, Typhoon Morakot produced a record-breaking 2777 mm of accumulated rainfall over four days, exceeding the previous record of 1736 mm (Typhoon Herb – 1996; Ge *et al.*, 2010).

Record-breaking rainfall produced by the typhoon is attributed to multiple factors. Morakot received a substantial moisture flux from the nearby Tropical Storm Goni (Zhang *et al.*, 2010; Chien and Kuo, 2011; Wu *et al.*, 2011; Xu *et al.*, 2011; Yen *et al.*, 2011), enhancing precipitation by 30% (Xu *et al.*, 2011). Additional moisture was provided by monsoonal circulation to the southwest of Morakot (e.g. Ge *et al.*, 2010; Hong *et al.*, 2010; Wu *et al.*, 2011; Hall *et al.*, 2012). Finally, precipitation was orographically enhanced by the Central Mountain Range (CMR) as the typhoon slowed while moving inland (Chien and Kuo, 2011; Ge *et al.*, 2010). In sum, the extreme precipitation produced by Typhoon Morakot resulted from an ideal convergence of meteorological factors, including monsoonal circulation, nearby tropical cyclones, and interactions with the CMR. Analysis of precipitation statistics extrapolated from smaller events have been used to argue for an ~200 year recurrence interval for an event like Morakot (Chu *et al.*, 2011); however others have cautioned that such extrapolations are not appropriate for the rare atmospheric conditions that occurred during Morakot (Ge *et al.*, 2010; West *et al.*, 2011).

The intense precipitation from Typhoon Morakot triggered 22 705 observed landslides in southern Taiwan and the Hengchung Peninsula (Lin *et al.*, 2011). Landslides occurred in areas with cumulative precipitation > 800 mm, which are located over much of our study area (Figure 2). Maximum landsilding occurred in the central and northern part of our study area (Figure 2C), with a few exceptions (note the northeastern most basin in Figure 2C). Landslides in the region visibly altered the geomorphology of local channels by introducing a large influx of sediment to streambeds (Figure 3). Based on previous studies exploring fluvial response to regional landslide events (Goswami, 1985; Pearce and Watson, 1986; Yanites *et al.*, 2010a; Li *et al.*, 2016), we can expect the impact of this event to propagate through the landscape, potentially influencing river morphology and flood inundation patterns for the coming years and decades. Our focus is to document such changes and consider the results in the context of propagating geomorphic hazards and the long-term geomorphic character of the Hengchung Peninsula in Taiwan.

Methods

We focus our analysis on 20 basins: 10 on the western side and 10 on the eastern side of southern Taiwan (Figure 1A). The basins cover a range of the topographic relief observed in the modern topography (Figure 1D). This provides an opportunity to compare channel geometries with different landslide inputs associated with Typhoon Morakot. We can also assess the impacts on long-term sediment supply in areas that experienced more and/or larger landslides to those that experienced fewer and/or smaller landslides over time. Additionally, by exploring both eastern and western basins, we can compare cross-orogen differences in geomorphic response. Rain gauges suggest the western side received more precipitation (Figure 2), and landslide concentration was highest where cumulative precipitation was also the highest (Lin *et al.*, 2011; Huang *et al.*, 2017).

We begin our analyses by first identifying spatial variations in hillslope and river steepness using the 30 m ASTER GDEM V2 (Tachikawa *et al.*, 2011). Hillslope gradient, relief, and channel steepness indices are considered, as these metrics are representative of the changes in topography across Taiwan and set the geomorphic framework on which the typhoon impacted erosion and sediment transport processes. Next, we measure channel width in each basin from the mountain front and upstream to where channel banks cannot be resolved on the imagery.

Channel slope

River profiles exhibit a scaling relationship, such that above some critical drainage area (Montgomery and

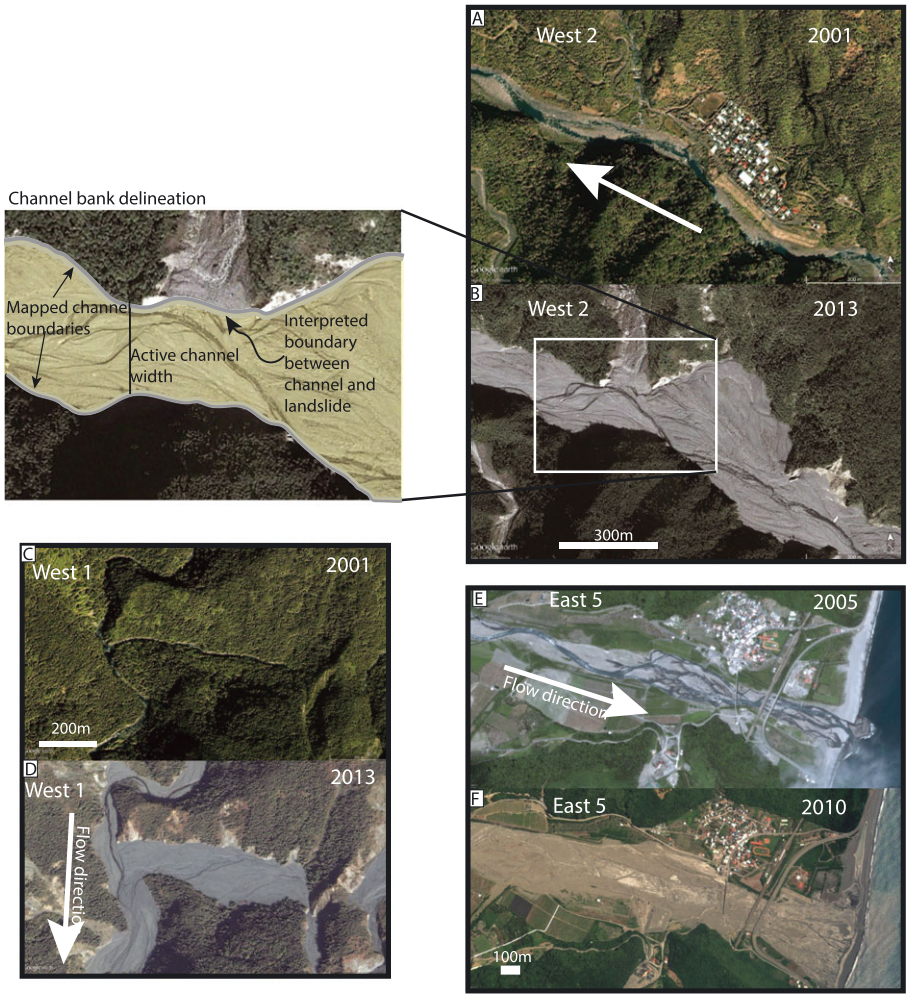

Figure 3. Examples of significant channel change following Typhoon Morakot. (A–B) Compare West basin 2 in 2001 (A) and 2013 (B). Inset shows and example of channel delineation. (C–D) Compare West basin 1 in 2001 (C) and 2013 (D). The 2001 image shows the limit of channel visibility for accurate delineation. (E–F) Compare East basin 5 in 2005 (E) and 2010 (F). [Colour figure can be viewed at wileyonlinelibrary.com]

Foufoula-Georgiou, 1993) slope varies as a power-law function of drainage (Flint, 1974; Wobus *et al.*, 2006a):

$$S = k_s A^{-\theta} \tag{1}$$

where S is slope, A is drainage area (in m^2), k_s is the steepness index ($m^{2\theta}$), and θ is concavity. The dimensions of k_s depend on the value of θ, and we have elected to calculate a normalized steepness index k_{sn} by using a reference concavity, θ_{ref} (Wobus *et al.*, 2006a):

$$k_{sn} = \frac{S}{A^{-\theta_{ref}}} \tag{2}$$

To compare channel slope at different drainage areas, we calculate a normalized steepness index by assuming θ_{ref} = 0.5. This is within the range of local θ in our study area and is consistent with theory of river incision processes in tectonically active, eroding river systems (Snyder *et al.*, 2000). Using a reference concavity provides a simple, straightforward metric to compare channel slope, fixed for the impact of changing drainage area, to our channel width measurements. As outlined later, we will also normalize channel width in a similar approach. For this reason, we rely on the slope-area method rather than slope-integral methods of channel steepness (Perron and Royden, 2013). We note, however, that the general pattern and magnitudes of steepness generated with either method is similar (Chen and Willett, 2016) (Figure 1B).

Hillslope morphology

Hillslope erosion processes supply sediment to river channels, and rates of hillslope erosion increase with hillslope gradient (Culling, 1960; Roering *et al.*, 2001; Montgomery and Brandon, 2002). In steep landscapes, the relationship between hillslope erosion and gradient is non-linear because of the strong sensitivity of landslide susceptibility to hillslope gradient (Larsen and Montgomery, 2012). This manifests in the observation that a large change in hillslope erosion processes is associated with an almost imperceptibly small increase in gradient when hillslope gradient approaches material strength limits (Schmidt and Montgomery, 1995). This phenomenon has led to the development of the threshold hillslope concept (Burbank *et al.*, 1996; Montgomery, 2001). Although erodibility contrasts can cause spatial trends in hillslope gradients to be unrepresentative of the trends in erosion rates (Riebe *et al.*, 2000), the relatively uniform lithology of the study area (Wiltschko *et al.*, 2010) should minimize differences in erodibility and promote the use of hillslope gradients as a proxy for erosion rates and long-term sediment supply.

We calculate two hillslope metrics, gradient and relief, to map both patterns in long-term sediment supply to river channels and landslide potential. Calculations were done using

TopoToolbox v2 (Schwanghart and Kuhn, 2010; Schwanghart and Scherler, 2014). The code calculates slope by quantifying the maximum elevation drop over a 3 × 3 pixel window surrounding each 30 m pixel. Relief is calculated across the landscape using maximum differences in elevation within a 1 km radius centered on each pixel. We consider mean and median values for both hillslope gradient and relief, as well as the values representing the 90th and 95th percentiles of each metric's distribution.

Quantifying channel width

Active channel boundaries were delineated from satellite images available in Google Earth. To quantify changes, we delineated channel boundaries in images taken in years before and after Typhoon Morakot (Table I). High quality imagery following Morakot are available for all basins, but only a subset of basins also included pre-Morakot imagery of sufficient resolution to confidently map channel margins. Channel extents were interpreted to include visible surface water, as well as alluvium surfaces within the vegetated banks, typically composed of gravel or sand bars that are active during typhoon flooding (Figure 3). Both field and remote evidence indicate that active bedload transport occurs within the channel extents delineated by our method. We ignored reaches with clear anthropogenic impacts such as dams, agriculture fields (e.g. watermelon farms), and other distinct channelization engineering. Channel polygons were analyzed using the ChanGeom processing software (Fisher *et al.*, 2013). Measuring channel width in Taiwan is facilitated by the stark contrast between active channel sediments and vegetation. In fact, the original developers of ChanGeom used a dataset of central Taiwan (Yanites *et al.*, 2010b) as an early test of their methodology (Fisher *et al.*, 2013). To further test the accuracy of this approach, we compare remote observations with 14 field-measured widths obtained with a LaserTech rangefinder (1-cm precision) in May of 2015. Active flood width in the field was chosen based on visible high-water marks such as flood debris, evidence of active scour, and mineralization on fresh bedrock surfaces.

In most mountainous river systems, channel width increases with drainage area (Montgomery and Gran, 2001; Wohl and David, 2008; Yanites and Tucker, 2010). The strength of the relationship between area and width, however, varies for a number of reasons, including rock-type (Allen *et al.*, 2013; Spotila *et al.*, 2015), climate (Finnegan *et al.*, 2005), sediment supply

Table I. Data for the 20 basins analyzed as part of this study. See text for further description of variables

Basin name	Distance from southern tip	Mean k_{sn}	Median k_{sn}	Mean 1 km relief	Median 1 km relief	Mean slope	Median slope		Year of image	k_w	b
West 1	91	226	215	445	434	57.4	53.3	post-Morakot	2011	4.91E-04	0.60
								pre-Morakot	2001	1.44E-03	0.48
West 2	84	307	284	479	462	61.8	56.6	post-Morakot	2014	2.79E+00	0.20
								pre-Morakot	2001	1.56E-02	0.43
West 3	76	279	260	436	420	56.2	51.8	post-Morakot	2011	4.12E-01	0.25
								pre-Morakot		—	—
West 4	64	269	241	501	489	61.4	56.5	post-Morakot	2011	3.35E+00	0.21
								pre-Morakot		—	—
West 5	54	231	226	447	442	56.8	53.3	post-Morakot	2014	1.69E+00	0.28
								pre-Morakot		—	—
West 6	46	192	196	416	414	55.6	53.3	post-Morakot	2014	2.61E-02	0.39
								pre-Morakot			
West 7	41	160	163	352	342	50.0	47.1	post-Morakot	2014	2.11E+01	−0.04
								pre-Morakot		—	—
West 8	35	170	153	360	361	50.0	47.1	post-Morakot	2011	1.38E-04	0.74
								pre-Morakot		—	—
West 9	29	96	101	268	277	39.4	37.7	post-Morakot	2014	4.89E-06	0.85
								pre-Morakot		—	—
West 10	16	73	62	232	225	36.2	33.3	post-Morakot	2014	1.93E-05	0.79
								pre-Morakot	2007	6.95E-05	0.77
East 1	96	283	269	470	468	60.2	56.5	post-Morakot	2014	1.42E+01	−0.06
								pre-Morakot	2006	4.27E+00	0.10
East 2	89	269	233	414	411	53.5	50.0	post-Morakot	2014	2.68E+00	0.12
								pre-Morakot	2005	*insufficient data*	
East 3	77	281	248	450	440	57.3	53.3	post-Morakot	2011	2.19E+04	−0.31
								pre-Morakot	2001	7.17E-01	0.23
East 4	70	270	245	462	446	59.3	54.2	post-Morakot	2011	4.47E-03	0.52
								pre-Morakot	2005	5.64E+00	0.15
East 5	62	218	203	396	389	52.5	49.4	post-Morakot	2013	1.87E+00	0.19
								pre-Morakot	2005	3.19E-01	0.27
East 6	51	177	178	363	366	50.0	47.1	post-Morakot	2011	3.63E-01	0.34
								pre-Morakot			
East 7	43	124	114	268	262	39.5	36.6	post-Morakot	2011	3.87E-04	0.66
								pre-Morakot			
East 8	31	62	61	199	209	33.1	30.6	post-Morakot	2014	4.57E-01	0.31
								pre-Morakot			
East 9	23	65	40	181	178	29.3	26.6	post-Morakot	2011	8.11E-05	0.72
								pre-Morakot		3.42E-07	1.20
East 10	8	46	44	169	158	24.9	23.3	post-Morakot	2014	1.42E-02	0.37
								pre-Morakot	2007	3.49E-03	0.43

(Finnegan *et al.*, 2007; Yanites and Tucker, 2010), erosion rate (Finnegan *et al.*, 2005; Whittaker *et al.*, 2007), and channel roughness (Goode and Wohl, 2010). We regress channel width and drainage area data to quantify the strength of the area–width relationship:

$$W = k_w A^b \tag{3}$$

where W is channel width (in meters), k_w is the channel width scaling factor (m^{1-2b}), A is upstream contributing drainage area (in m^2), and b is an exponent. Note the similarities between Equations (3) and (1).

The scaling relationship in Equation (3) can also be used to calculate the relative wideness of a river channel by accounting for the tendency for channels to widen with increasing drainage area. Following Yanites and Tucker (2010) and Allen *et al.* (2013), we normalize channel width by drainage area to yield channel wideness, k_{wn}, for comparison among different sized drainages:

$$k_{wn} = \frac{W}{A^b} \tag{4}$$

We use a value of 0.37 for b, which is the median value of all drainage basins (see Results later and Table I). The approach allows the comparison of channel width for different drainage basin sizes as well as different values of steepness (e.g. Equation (2)).

Normalizing steepness by wideness

The stream power erosion model (Whipple and Tucker, 1999) is often used as a theoretical basis for explaining channel steepness in tectonically active landscapes (Snyder *et al.*, 2000; Wobus *et al.*, 2006a). The data presented here provides a means to test this model as well as many of the assumptions behind it. Specifically, many approaches of the stream power model, assume channel width only scales with drainage area and is therefore not explicitly accounted for in channel steepness patterns. One can account for non-uniform width–area scaling by normalizing channel steepness by channel wideness, k_{wn} (Equation (4)). First, we start from the assumption that bedrock incision rates (E) scale with unit-stream power, ω, raised to a power, a (Whipple and Tucker, 1999):

$$E = k_b \omega^a = k_b \left(\rho g \frac{Q_w}{W} S \right)^a \tag{5}$$

where k_b is the lithology dependent erodibility value, a is a positive constant that is related to the dominant process of erosion (Whipple *et al.*, 2000), Q_w is water discharge (in $m^3\ s^{-1}$), W is channel width (in meters), and S is stream gradient. Frequently, drainage area is substituted for channel width, W, with Equation (3). Thus, Q_w is often assumed to be a power-law function of drainage area (Whipple and Tucker, 1999):

$$Q_w = k_Q A^c \tag{6}$$

where k_Q is a constant related to precipitation (in $m^{3\text{-}2c}\ s^{-1}$) and c is a unitless exponent typically ranging from 0.7 to 1 (Whipple and Tucker, 1999). These relationships are combined with Equation (5), yielding:

$$S = \frac{k_w}{k_Q \rho g} \left(\frac{E}{k_b} \right)^{1/a} A^{b-c} \tag{7}$$

Note that $b - c$ should equal θ. River incision, E, is often assumed to equal the rate of rock-uplift, U, in Equation (7), but since southern Taiwan is a growing orogen, we do not make this assertion.

Equation (7) is the slope–area scaling often used in tectonic geomorphology studies and all the constants are lumped into a bulk erodibility value often denoted as K. Essentially, the approach assumes that variation in channel steepness reflects variations in fluvial shear stress (or unit stream power) as a proxy for erosion potential. Recent studies have shown that variations in k_Q has a significant influence on channel steepness, requiring precipitation based scaling of channel steepness to appropriately map shear stress (Gasparini and Whipple, 2014). It is our aim to test if unaccounted variations of channel width can similarly muddle interpretations of channel steepness. If the values of θ_{ref} and b effectively remove any dependence of both k_{sn} and k_{wn} on drainage area such that $k_s \sim k_{sn}$ and $k_w \sim k_{wn}$, then channel steepness can be normalized as

$$\frac{k_{sn}}{k_{wn}} = \frac{1}{k_Q \rho g} \left(\frac{E}{k_b} \right)^{1/a} \tag{8}$$

Normalizing steepness by wideness may therefore highlight the roles of other factors, such as the erodibility factor (k_b) or climate and hydrology factor (k_Q) on the pattern of unit stream power. The ratio represents a proxy for unit stream power that allows for systematic changes in channel width. This allows for changes in slope and/or width at a given drainage area to drive changes in river incision. While our analysis of this ratio is focused on the along strike patterns, this derivation is also relevant in exploring downstream variations in erosion potential. Future work exploring downstream patterns in incising rivers could be insightful towards understanding trade-offs between channel width and slope adjustments in these systems.

The approximation allows for uniform river incision potential maintained by equivalent adjustments in both slope and width (e.g. both increase). In other words, an increase in slope does not have to equal an increase in erosion potential (i.e. shear stress or unit stream power) if channel width also increases. Because channel width is sensitive to sediment loading and transport (Finnegan *et al.*, 2007; Turowski *et al.*, 2007; Yanites and Tucker, 2010), wideness-normalized steepness can aid in understanding the balance of channel and hillslope processes and how this balance varies spatially with tectonic and climatic drivers. For example, some river systems in tectonically active regions appear to be limited by the ability to remove sediment overlying bedrock to allow erosion processes to occur (Johnson *et al.*, 2009; Yanites *et al.*, 2011). In these settings, channel morphology maximizes sediment transport capacity and is predicted to manifest in steeper yet wider channels (Turowski *et al.*, 2007; Yanites and Tucker, 2010), whereas detachment-limited systems are expected to narrow as rivers steepen (Finnegan *et al.*, 2005; Wobus *et al.*, 2006b; Yanites and Tucker, 2010). By mapping both steepness and wideness, we aim to test such predictions.

Results

Geomorphic context

The general patterns of channel and hillslope gradients are consistent with the southward propagation of the Taiwanese orogen (Figures 1 and 4). Channel steepness values are lowest in the south and generally increase to the north (Figures 1B and 4B) (e.g. Wiltschko *et al.*, 2010; Chen and Willett, 2016). There is an across-orogen pattern of maximum steepness near the core of the range that decreases toward the mountain front

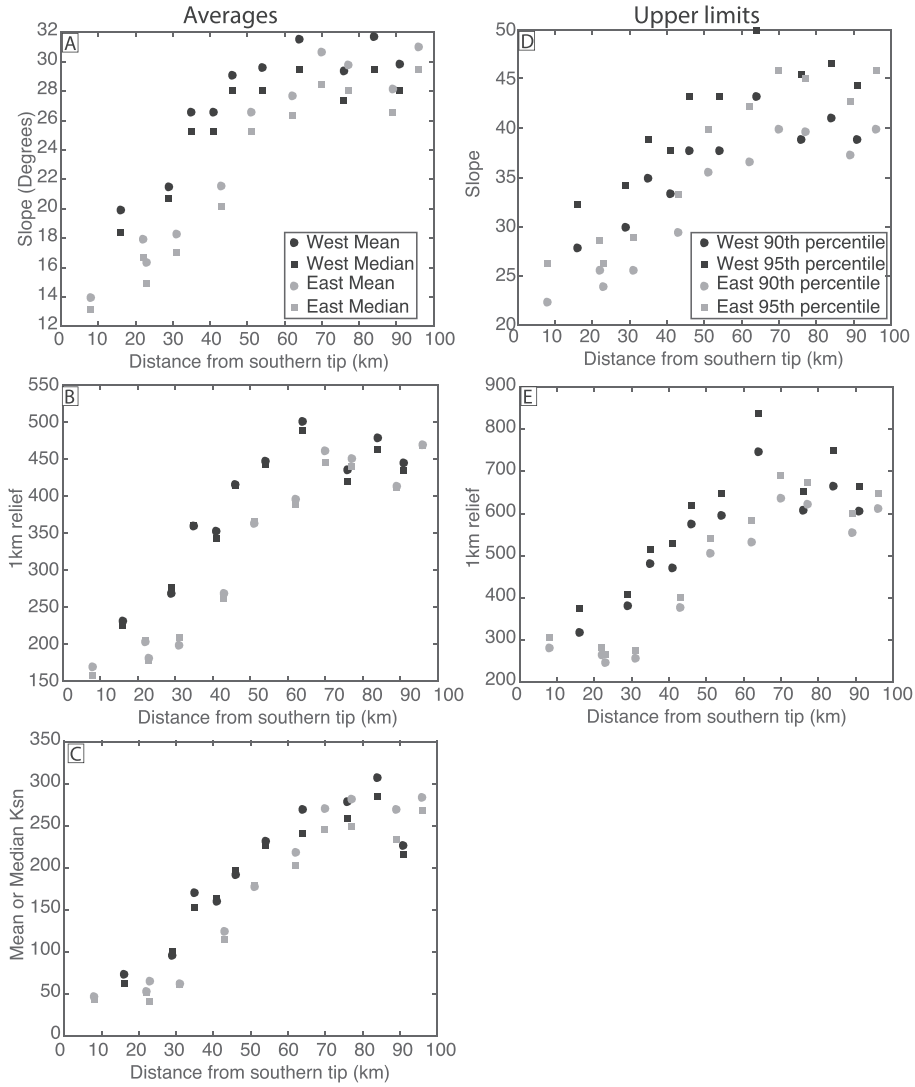

Figure 4. Hillslope statistics along strike. Average hillslope gradient (A), 1 km relief (B), and channel steepness (C) with distance from southern tip of Taiwan for the 20 basins studied. The 90th and 95th percentile for slope (D) and relief (E) are also plotted.

on both sides of the orogen (Figure 1B). This is especially prevalent in the central and northern part of the range (Figures 1 and 5). A concavity of 0.5 appears to remove most of the drainage area dependence on slope although there appears to be correlation between k_{sn} and drainage area for some basins in the central to northern basins suggesting a higher concavity (Figure 5).

Hillslope morphology metrics follow a pattern similar to that of steepness, with both gradient and relief increasing from south to north, achieving local maximums at the core of the range (Figures 1C–1D and 4). Mean and median values of hillslope gradient and relief increase steadily from the southern tip to ~60 km (Figures 4A and 4B), where mean and median values become more uniform. The basins at the northern extent of the study area may be slightly less steep, which is most evident in the relief data (Figure 4B); however, the difference is quite small. The 90th and 95th percentiles reveal the spatial pattern of the steepest hillslopes in each catchment (Figures 4D and 4E). These values follow a similar trend as average hillslope metrics (i.e. a south to north increase in hillslope gradients and relief). One difference, however, is that the 90th/95th percentiles of 1 km relief (Figure 4E) are lower in the basins at the northern end of the study area. The leveling off (or slight decrease) in hillslope gradient (Figure 4D) may indicate a threshold hillslope condition (Burbank *et al.*, 1996; Montgomery, 2001). We note that the digital elevation model (DEM) resolution influences the absolute values of slope, especially in steep terrain (Mukherjee *et al.*, 2013). Nonetheless, assuming hillslope gradient and relief (Figures 1C and 1D) reflects relative differences in sediment supply to channels, we can expect that long-term (centennial- to millennial-timescale) sediment supply from hillslopes to channels has a strong spatial variation across the landscape, which is corroborated by cosmogenic nuclides (Fellin *et al.*, 2017). We also anticipate landslide susceptibility to closely follow this pattern of hillslope morphology.

Channel width

We compare digitized channel width and field-based measurements (Figure 6). In general, the relationship between digitized and field measurements closely follows the 1:1 line (the average misfit is $< 10\%$ of the remotely measured width). The largest outliers are locations with the widest field measured widths, suggesting that channel width for wide rivers is either underestimated by remote methods or overestimated by field measurements, respectively. Although either scenario is possible, we argue that our field measurements likely overestimate width, as the river stage during the field campaign limited our ability to precisely locate high water marks on both sides of the river. Consequently, far-field estimates of flood height made for the opposite banks were based on the first observations of

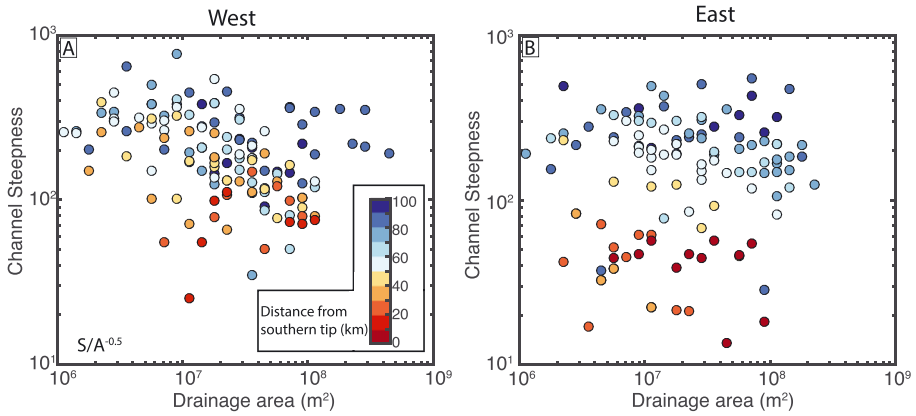

Figure 5. Channel steepness versus drainage area along west (A) and east (B) sides of study area. Steepness calculated with a concavity of 0.5. [Colour figure can be viewed at wileyonlinelibrary.com]

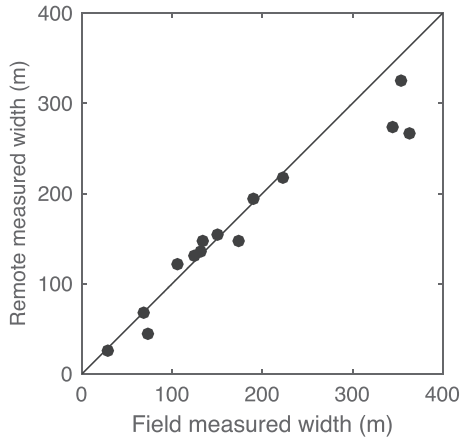

Figure 6. Test of remote width measurements. Field measured width is consistent with remote width estimates.

non-inundated locations, which is a conservative (i.e. maximum) estimate of bankfull width. Nonetheless, the strong relationship observed in Figure 6 justifies that the approach taken here generates reliable data that are consistent with field measurements.

Spatial variations in channel width

Our results show that even in a location with similar lithology and climate, channel width is quite variable along strike. Figure 7 shows averages of channel width versus drainage area, with the averages centered on 30 equally log-spaced area bins between 10^6 and 10^9 m^2. The temporal changes in channel width (i.e. changes along strike before and after Morakot) also vary significantly along strike (compare squares and circles in Figure 7). Prior to the typhoon, the narrowest channels on the eastern side of the study area were located in the southernmost basin (Figure 7B). On the western side of the study area, the narrowest channel widths were located in the northernmost basin (Figure 7A). In either case, the widest pre-Morakot basins (squares, Figure 7) were in the central to north-central parts of the study area.

We also illustrate the N–S trend by plotting width versus distance from the southern tip for a given drainage area (Figure 8). For example, at ~22 km^2 and ~35 km^2, channel width is relatively narrow at the southernmost basins. The width increases northward until ~70 km from the southern tip before remaining constant or decreasing slightly (Figure 8). The maximum

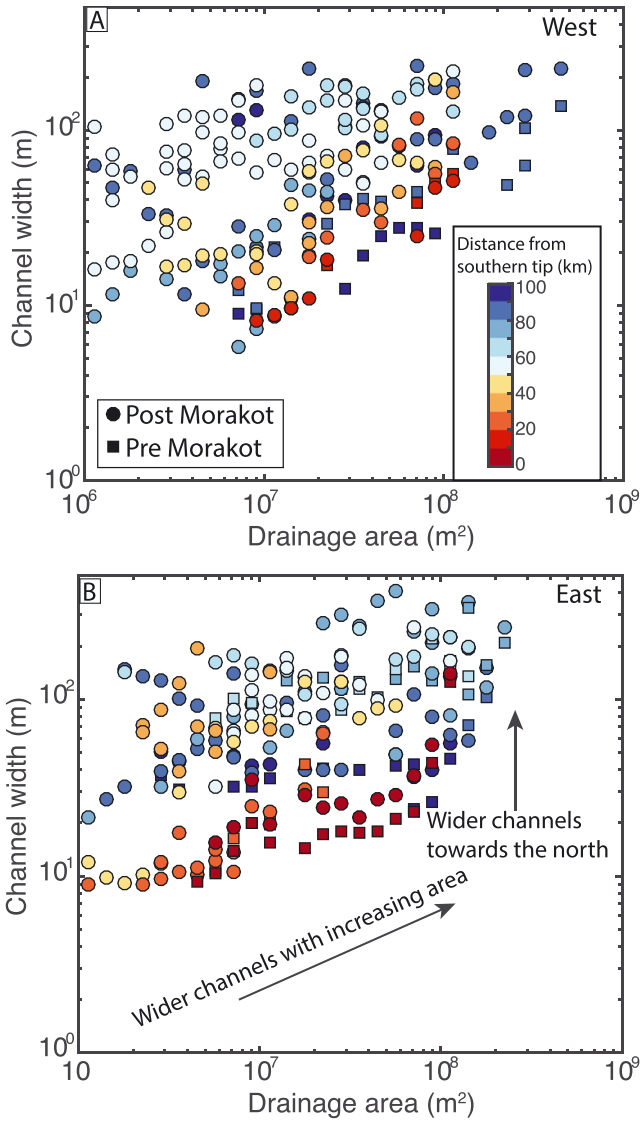

Figure 7. Relationship between channel width and drainage area for basins studied here. Bin averaged channel width is plotted for both western channels (A) and eastern basins (B). Points are colored by distance from southern tip of Taiwan. The change in channel width from pre- to post-typhoon is illustrated in Figure 10. [Colour figure can be viewed at wileyonlinelibrary.com]

difference results in a seven-fold increase in channel width from south to north. Note that not every basin is represented in these plots. The reason is that the data show log-bin averages

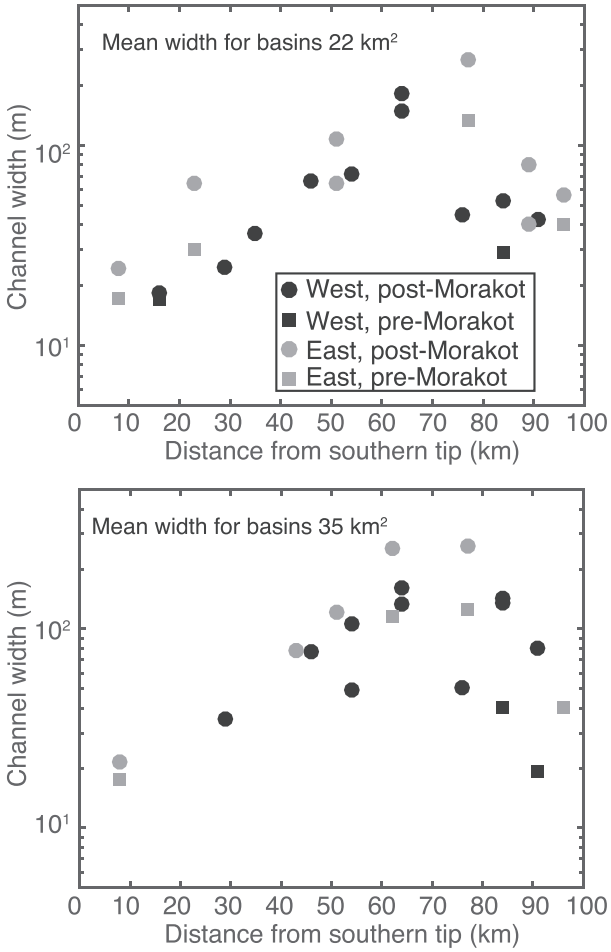

Figure 8. Channel width along strike for the 22 km^2 (A) and 35 km^2 (B) log-binned average drainage areas.

centered on 22 km^2. We note that some basins do not have a measured width within the plotted area-bins as a consequence of discrete changes in drainage area at tributary junctions.

Normalized channel wideness allows a comparison of channel widths at any drainage area. Although there is considerable variation in the exponent between width and area (*b*, Table I), the median value for all the basins (0.37) removes the drainage area dependence in most basins (Figures 9A and 9B). Nevertheless, there is still a clear trend along strike (Figure 9) where the southern channels tend to be the narrowest and central to north-central channels are the widest. Comparing channel wideness and steepness results in distinct clustering of drainage basins suggesting that the relationship between width and slope is more complicated than suggested by simple scaling arguments (Finnegan *et al.*, 2005) that predict an inverse relationship between width and slope when drainage area effects have been accounted for.

Temporal variation in width: response to Morakot

Note the observed temporal changes in channel width are mostly due to aggradation. In many locations, this aggradation is on the order of 10^0 to 10^1 m. In the most extreme locations, this included the filling of inner channels, subsequently spilling sediment onto adjacent terraces (Figure 3). As such, the changes influence the efficacy of geomorphic processes such as sediment transport capacity and bedrock erosion. In fact, in many cases, bedrock erosion on the channel bed has probably stopped until significant sediment evacuation occurs.

The spatial trend in channel width was accentuated by changes resulting from Typhoon Morakot, which amplified widening in rivers in the central and northern basins with the exception of basin East 1 (see Figure 1A for basin numbers), which experienced limited Morakot associated landsliding (Figure 2

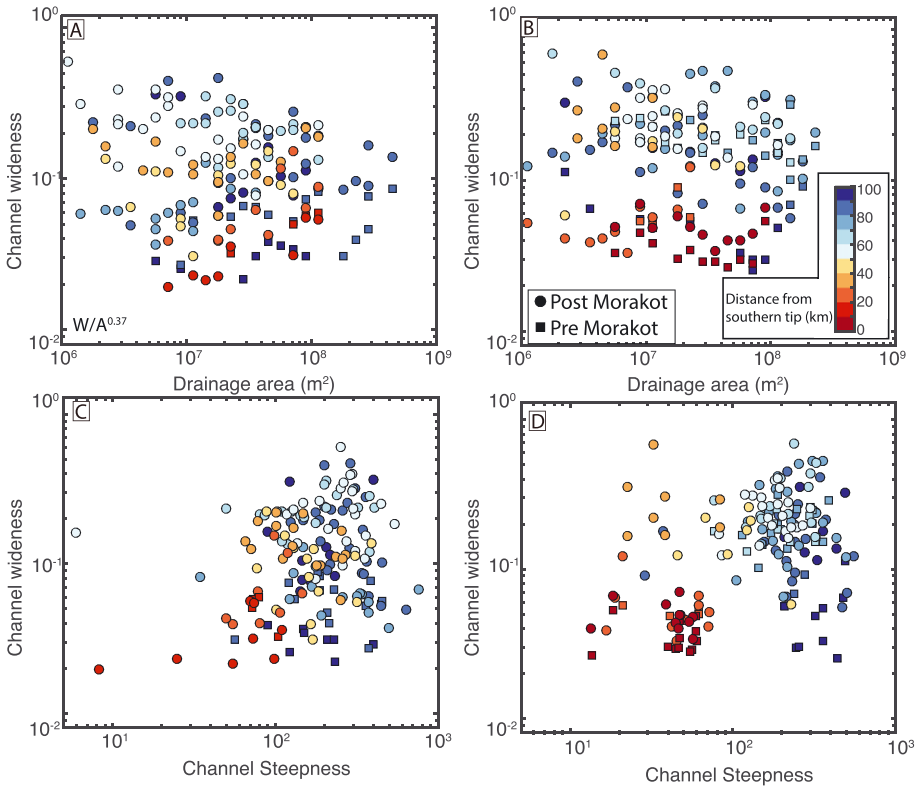

Figure 9. Channel wideness versus drainage area (A, B) and steepness (C, D) for the west (A, C) and eastern (B, D) sides. Points are colored by distance from southern tip of Taiwan. [Colour figure can be viewed at wileyonlinelibrary.com]

C). Prior to the typhoon, channels in the central (e.g. basins West and East 3–4) part of the study area were ~3–10 times wider than the channels in the south, in the years following the typhoon, some of the channels widened to > 10 times greater than the southern counterparts (Figure 8). Many channels in the central to northern part of the study site had increased widths of two- to three-fold, with some exceptional cases increasing width by an order of magnitude or more (Figure 10). An exception to this trend is basin East 1, which had little difference between pre- and post-typhoon width estimates. Among the western basins, West 1 and 2 experienced the most change following Typhoon Morakot (Figure 10), with basin West 1 having up to a 14 times increase in width. The maximum width change in basin West 2 occurred in headwater streams. The largest increases in width on the eastern side occurred in basins East 3 and 4 having 50–300% increases in width. In summary, significant changes in channel morphology were greatest among central (the lightest blue in Figure 10) and northern basins (dark blue in Figure 10) in the west, while similar significant changes in the east were restricted to central basins (East 3 and 4) where landsliding was most intense (Figure 2C).

Although visual observations of channel morphology suggest that the largest temporal changes occurred in headwater streams, the resolution of pre-Morakot imagery prevented delineation of many of these narrow headwater channels. This is well illustrated in Figure 7 where wide, post-Morakot channels exist in many of the central and northern basins, while we were not able to resolve the pre-Morakot channel width. Therefore, the lack of data in the upper left of Figure 10 (i.e. the lack of squares for drainage areas less than 7×10^6 m^2) is not because channels with lower drainage areas remained unchanged, but rather, because pre-Morakot imagery was unable to resolve these channels. Nevertheless, the very wide channels at small drainage areas of the post-Morakot data (Figure 7) should be taken as evidence of substantial channel change in these headwater streams. Channels widened at large drainage areas in the northern and central basins as well, but note the relative change was smaller than locations upstream (Figure 10). The southern channels drain topography with generally low slopes and relief (Figure 1), and these channels had minimal changes in width after the typhoon (Figure 10).

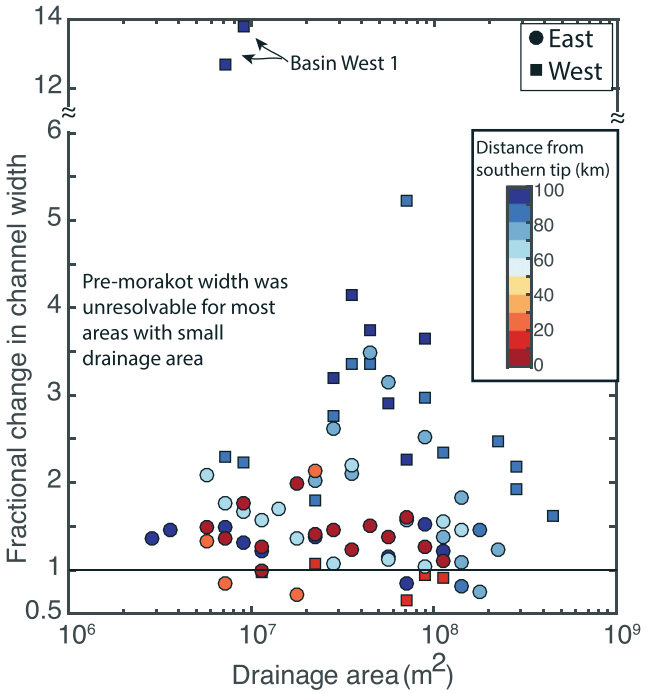

Figure 10. Change in channel width following Typhoon Morakot at different drainage areas.Note the broken *y*-axis between six- and 12-fold change in width. The lack of data for small areas is because channel width was unresolvable for small basins in pre-Morakot imagery, and not because there was not significant change in these areas. [Colour figure can be viewed at wileyonlinelibrary.com]

Wideness-normalized steepness

Normalizing channel steepness with channel wideness tests how well the channel steepness pattern reflects variations in unit stream power in southern Taiwan (Figure 11). Patterns in channel steepness showed a clear N–S trend (Figure 5); however, after correcting for channel wideness, this trend is not as apparent (Figure 11). The two northernmost basins (East and West 1) remain as the highest apparent erosion potential, but other basins with high steepness (Figure 4B) and channel width (Figures 7 and 8) in the central to northern part of the study area do not appear to have as high of an erosion potential (Figure 11). This pattern is consistent between both pre- and post-typhoon channel widths (squares versus circles in Figure 11), especially for the east side, suggesting this pattern of limited unit stream power variation is persistent in the southern Taiwan landscape. The lack of pre-Morakot imagery on the west side limits any conclusions on the persistence of this pattern.

Discussion

The spatiotemporal variability of channel morphology indicated by our results has a number of implications ranging from

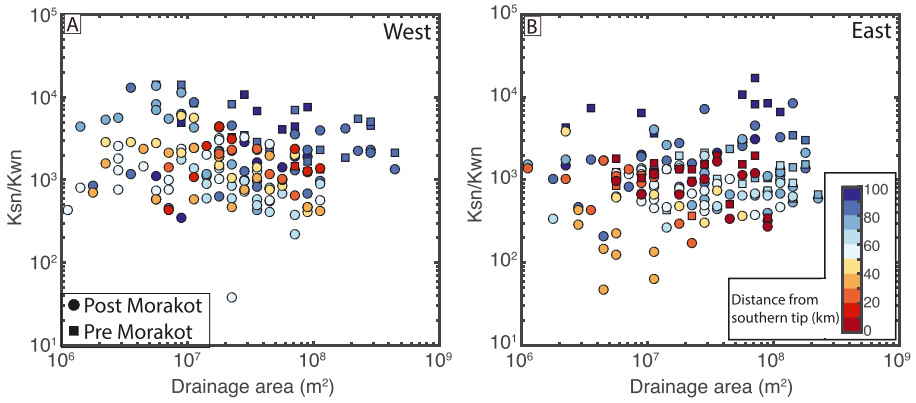

Figure 11. Channel steepness corrected for wideness at different drainage areas for western (A) and eastern (B) basins. Colors indicate distance from southern tip of Taiwan. [Colour figure can be viewed at wileyonlinelibrary.com]

short-term hazard mitigation to long-term tectonic geomorphic interpretation of channel morphology. Specifically, the observational record of dynamic river response to a large-magnitude, regional landslide event provides key insights to the dynamics of river systems in steep, landslide-prone landscapes over a range of timescales. Observations reveal high-magnitude hazards that have a cascading effect throughout fluvial systems of Taiwan, including channel aggradation and mobility. Furthermore, these hazards will likely impact riverside communities for decades to come. From a long-term perspective, the spatial variability observed in pre- and post-storm channel widths suggests that channel width is strongly influenced by sediment supply from hillslope processes. Finally, our results indicate that channel steepness observations alone likely overestimate variations in stream power and shear stress along this topographic gradient.

Cascading hazards and landscape records

An important implication of the observed landslide driven channel change (Figure 3) is the potential for continued impacts on flood inundation patterns from significant in-channel aggradation (e.g. Stover and Montgomery, 2001; Chen and Petley, 2005; Lane *et al.*, 2007). Figure 12 illustrates a conceptual model and shows photographic evidence of how the propagation of this landslide material influences flooding and associated hazards. As aggradation fills the channel bottom (Figure 12), the stage for a given water discharge will rise due to decreases in channel conveyance (i.e. the cross-sectional area of the inner channel). Consequently, the frequency of flooding outside of the channel banks will increase and threaten infrastructure built when the river had a larger cross-sectional area to convey the water discharge (e.g. Figures 3F and 12). In Figure 12B, a channel on the left side of the image has been evacuated in an attempt to limit flooding of this abandoned town. The duration of the impacts on flood inundation patterns is a function of sediment evacuation timescales, which also influence the lasting impact of events like Morakot on the long-term landscape evolution (see discussion later). Assuming that river response to the sediment delivery induced by Morakot is similar to the response to the Chi-Chi earthquake (1999), which also generated tens of meters of river aggradation (Chen, 2009; Hsu *et al.*, 2010), the sediment evacuation timescale will likely be on the order of decades to centuries (Yanites *et al.*, 2010b). Such a response timescale would be similar to other regions, such as New Zealand (Pearce and Watson, 1986) and the Himalaya (Goswami, 1985). Events such as regional landsliding thus add a non-stationary component to flood stage records, and should therefore be considered by stakeholders concerned with flooding risks in regions susceptible to such events.

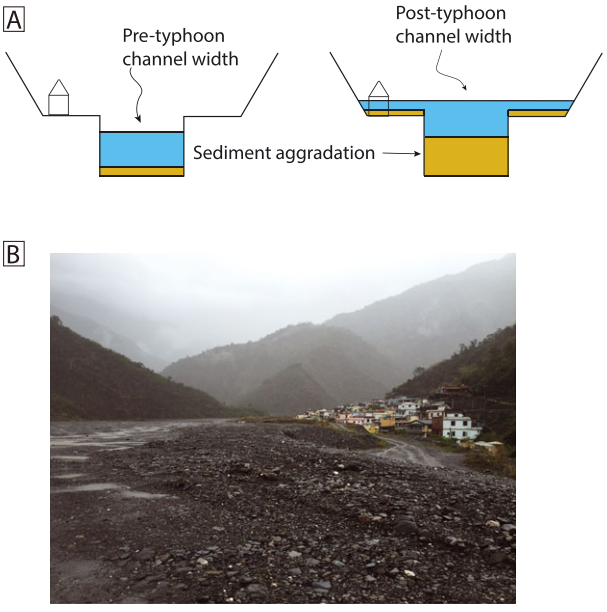

Figure 12. Illustration and image of the effects of cascading hazards in southern Taiwan associated with Typhoon Morakot. The landslide debris aggrades river beds as is propagates through the landscape, lowering channel conveyance and increasing flood risk (A). Many locations along the rivers in the north and central parts of the study area have been abandoned due to high flooding risk (B). The photograph was taken in May of 2015. [Colour figure can be viewed at wileyonlinelibrary.com]

The observed channel widening and aggradation is spatially variable. Landslides occurred on steep hillslopes that received $>$ 800 mm of rain during the storm (Lin *et al.*, 2011). Only in these basins has significant channel change occurred (Figure 10). Other steep basins experienced very little channel change if rainfall was limited, such as basin East 1 in the north-eastern part of our study area, which experienced over all less landsliding (Figure 2C). Such observations confirm the observed changes in channel morphology are a result of cascading hazards and are not driven by a longer-term trend in climate driven variations in sediment supply or water discharge (e.g. Montgomery *et al.*, 2014) which should affect all basins in the region. These observations reveal significant spatial variability in cascading hazards, highlighting that predictions of hazard potential will be event and site specific.

Finally, the channel response to this event has significant potential to create a lasting terrace record. The magnitude of observed channel change due to aggradation is quite significant in some of the basins, such as West 1 (Figure 3). Paleo-landslide events responsible for terrace formation have been documented in previous studies, although those studies attribute the terraces to seismically induced landslides (McPhillips *et al.*, 2014; Schwanghart *et al.*, 2016). An implication of our observations is that individual, large magnitude atmospheric events, such as tropical cyclones, may be capable of generating lasting terraces due to the cascade of geomorphic processes associated with regional landsliding. The record, however, will be quite spatially variable as nearby basins responded differently depending on the specifics of precipitation magnitudes across the landscape during the event (e.g. basin East 1 experienced little change). Such spatial variability may be a way to distinguish between seismic versus precipitation driven events. Further observations of channel response to landslides driven by different mechanisms are needed to fully understand the terrace record of extreme events.

Hillslopes control channel morphology

The spatial trend in channel width along strike of the growing Taiwan orogen suggests a dynamic coupling between hillslope and river processes. Previous theoretical and modeling approaches have suggested that channel width has a negative relationship with slope and erosion rates (Finnegan *et al.*, 2005; Wobus *et al.*, 2006b; Turowski *et al.*, 2009). This explanation alone cannot explain our data (Figure 9). Instead, our data show that the wider channels tend to occur where channel steepness (and hillslope gradient) are high with a few noted exceptions. This trend exists in the data both prior to and following the aggradation associated with Typhoon Morakot (Figures 7 and 8) suggesting it is not a transient feature of the landscape. We interpret this to indicate that sediment supply

is a strong control on bedrock channel width as documented in experimental channels (Finnegan *et al.*, 2007) and predicted theoretically (Turowski *et al.*, 2007; Yanites and Tucker, 2010).

Events that impact the sediment budget for a significant period, such as Morakot or large earthquakes, may be the reason that sediment is a dominant control on river dynamics in a rapidly uplifting environment such as Taiwan. Many channels in the north-central part of the study area have an excess of sediment covering and protecting the underlying bedrock (Figure 3), yet the Hengchung Peninsula is eroding at relatively high rates over millennial and longer timescales (Fuller *et al.*, 2006; Chen *et al.*, 2015; Fellin *et al.*, 2017). This requires significant variability in sediment cover in this landscape, which has been suggested for rivers in central Taiwan as well (Yanites *et al.*, 2011). As in the case for short-term hazards, understanding the timescale of this change is therefore an important future step in understanding the spatiotemporal dynamics of this landscape. If events such as Morakot occur with a frequency that is comparable to the evacuation timescale, then removal of landslide material may be a limiting factor on erosion potential in such landscapes.

The estimated 200-year recurrence interval (Chu *et al.*, 2011) and potential for multiple decade to century timescale in evacuation would suggest that sediment transport and bedrock exposure are dominant mechanistic controls on river morphology in this landscape. Recent studies have suggested that the fluvial response timescale of evacuating landslide material is much shorter (e.g. 5–25 years to remove 50% of the material) than previous estimates based on a model of dynamic channel adjustment to an individual landslide (Croissant *et al.*, 2017b). Field (Figure 12) and remote (Figure 3) observations suggest continued or sustained aggradation well beyond the event, rather than narrowing as suggested by Croissant *et al.* (2017b), suggesting the evacuation of Typhoon Morakot landslides is on the longer end of the scaling analysis. This is likely due to steeper channels in the headwaters oversupplying the downstream reaches with sediment, thereby lowering local rates of landslide evacuation. Further study observing the fate of this sediment and morphology (i.e. steepness and wideness) vary over time will provide important constraints towards understanding the temporal dynamics of river systems in landslide dominated landscapes. Specifically, the observations will provide insight into how multiple pulses of sediment into a mountain river may interact while the material is evacuated (Cui and Parker, 2005).

Consistent with the idea that sediment supply from landslide events lowers erosional efficiency on long timescales (Lague, 2010), steady-state theoretical approaches have suggested that in such scenarios, rivers with relatively high sediment loads should be wider and steeper than counterparts carrying less sediment (Turowski *et al.*, 2007; Yanites and Tucker, 2010). There are no long-term estimates on the frequency of regional landslide events in this area and as such, we cannot conclusively say if the evacuation of landslide material limits erosion; however, the clear relationship between hillslope morphology (and presumably landslide susceptibility) and wide, steep channels is consistent with the theoretical prediction that the river dynamics are dictated by sediment transport and bedrock exposure in these river systems. The role of regional landslide events versus continual sediment input from this steep landscape is an unresolved question. We note that in alluvial rivers sediment supply has a strong control on the lateral mobility of rivers which acts to further widen channels and valley bottoms (Wickert *et al.*, 2013). It is not clear if the sediment supply control on lateral mobility is as strong for coherent, bedrock banks. Physical arguments suggest that lateral erosion processes may be enhanced with increasing sediment supply (Nelson and Seminara, 2011); however, field evidence of lateral mobility suggests climate variability may play a dominant role (Stark *et al.*, 2010), which would suggest limited differences in lateral mobility among the basins in this study. Future work illuminating the physical controls on rates of channel widening and lateral mobility would be a fruitful exercise.

Patterns in orographic precipitation offer another potential explanation. It is documented that the higher parts of the Taiwan orogen receive higher annual precipitation, and rainfall intensity of individual events may be amplified by the topography (Chen *et al.*, 1990; Akaeda *et al.*, 1995; Chen and Chen, 2003). This greater precipitation and, presumably, water discharge, could explain the wider channels where the topography is steepest, which is in the core of the range (Figure 1). Observations along a single channel subject to significant orographic precipitation would predict relatively wider channels near the headwaters, with the wideness values decreasing in the downstream direction, as the river is further removed from the high precipitation area (if drainage area is a proxy for water discharge in Equation (4)). Such a prediction is consistent with the relatively low b values observed in the north-central channels (Table I), which indicate less variation of width with drainage area. However, observations of channel steepness run counter to such an explanation as one would expect lower steepness where precipitation is high which then increases toward the mountain front (e.g. Gasparini and Whipple, 2014). Instead, we observe channel steepness is a maximum where precipitation is high and then decreases towards the mountain front. If this was a detachment-limited system, with steepness set by higher rock-uplift and erosion in the core of the range, theoretical predictions suggest that channel width should have the inverse trend (i.e. relatively narrow in the headwaters and relatively wide at the mountain front). Therefore, it is difficult to reconcile these observations by variations in precipitation alone, though it might provide an important secondary control.

Instead, we propose the pattern is a manifestation of strong hillslope–channel coupling. The pattern in channel morphology suggests the rivers adjust to the sediment supplied by the upstream hillslopes. We note that although unit stream power or shear stress does not vary as strongly as implied by the channel steepness pattern (Figure 11), volumetric sediment transport capacity likely does. This is because channel width limits how wide the bedload area can be transported during storm events. Therefore, for a given shear stress and grain size, a wider (and steeper to maintain the same shear stress) channel will generate a greater volumetric bedload flux. The observation that channels are wider and steeper towards the north, even prior to the accentuation of the width pattern by Typhoon Morakot, suggests these channels are responding to increases in sediment supply over a range of timescales (e.g. both the extreme and background landslide events that occur during a range of rainfall intensities). The increase in sediment transport capacity from south to north is in response to the steeper hillslopes that develop as the Taiwan orogen grows from south to north. The greater transport capacity exposes bedrock to erosion more frequently, even though the hillslopes are generating sediment quite rapidly. This conceptual model suggests that the propagation of sediment generated from landslides through the fluvial system is a fundamental control in constructing the landscapes of southern Taiwan. It is this propagation of sediment that generates the cascade of hazards initiated by Typhoon Morakot and will likely impact the communities living along the streams for decades.

Conclusions

Documented spatiotemporal patterns of channel width along the Hengchung Peninsula in southern Taiwan suggest a strong coupling between hillslope and channel processes. Prior to

Typhoon Morakot, channels in the central to northern part of the study area were ~3–10 times as wide as rivers in the southern part of the area. Channels in the central to northern section of the study area were significantly impacted by Typhoon Morakot, which generated landslides in the basins that have both steep hillslopes and experienced high precipitation. The debris from these mass movements propagated through the landscape, aggraded riverbeds, and accentuated the spatial pattern in channel width. Rivers in these basins experienced a two- to 14-fold increase in the width of the active channel. The wider channels (for a given drainage area) tended to occur where channel steepness was also high, which is unexpected for a typical detachment-limited river model. In fact, we show that when accounting for the systematic, along-strike spatial differences in channel width, the variation in unit stream power is much less than what would be predicted from channel steepness patterns alone. Instead, we propose that river incision in this landscape is limited by the ability to expose underlying bedrock to erosive properties, and as such, the channel morphology is strongly influenced by the sediment supplied by the upstream hillslopes. This strong hillslope–channel coupling places a fundamental constraint on the long-term landscape evolution of this region and suggests that events like Morakot may influence patterns in topography through the initiation of a cascade of geomorphic processes and hazards that propagate through a landscape.

Acknowledgements—The authors thank Chun-Chieh Wu and Eric Hendricks for sharing the precipitation data and Cheng-Chien Liu for sharing the geographic information system (GIS) coverage of landslide area. Constructive comments from two anonymous reviewers and the Associate Editor greatly improved the manuscript. This work was supported by National Science Foundation grant EAR-1727736 to BJY.

References

Akaeda K, Reisner J, Parsons D. 1995. The role of mesoscale and topographically induced circulations in initiating a flash flood observed during the TAMEX project. *Monthly Weather Review* **123**: 1720–1739. https://doi.org/10.1175/1520-0493(1995)123%3C1720:TROMAT%3E2.0.CO;2.

Allen GH, Barnes JB, Pavelsky TM, Kirby E. 2013. Lithologic and tectonic controls on bedrock channel form at the northwest Himalayan front. *Journal of Geophysical Research: Earth Surface* **118**: 1806–1825. https://doi.org/10.1002/jgrf.20113.

Anderson SW, Anderson SP, Anderson RS. 2015. Exhumation by debris flows in the 2013 Colorado Front Range storm. *Geology*. https://doi.org/10.1130/G36507.1.

Budimir MEA, Atkinson PM, Lewis HG. 2014. Earthquake-and-landslide events are associated with more fatalities than earthquakes alone. *Natural Hazards* **72**: 895–914. https://doi.org/10.1007/s11069-014-1044-4.

Burbank DW, Leland J, Fielding E, Anderson RS, Brozovic N, Reid MR, Duncan C. 1996. Bedrock incision, rock uplift and threshold hillslopes in the northwestern Himalayas. *Nature* **379**: 505–510. https://doi.org/10.1038/379505a0.

Chen C-S, Chen W-S, Deng Z. 1990. A study of a mountain-generated precipitation system in northern Taiwan during TAMEX IOP 8. *Monthly Weather Review* **119**: 2574–2607. https://doi.org/10.1175/1520-0493(1991)119%3C2574:ASOAMG%3E2.0.CO;2.

Chen C-S, Chen Y-L. 2003. The rainfall characteristics of Taiwan. *Monthly Weather Review* **131**: 1323–1341. https://doi.org/10.1175/1520-0493(2003)131%3C1323:TRCOT%3E2.0.CO;2.

Chen C-Y. 2009. Sedimentary impacts from landslides in the Tachia River Basin, Taiwan. *Geomorphology* **105**: 355–365. https://doi.org/10.1016/j.geomorph.2008.10.009.

Chen CY, Willett S, West AJ, Dadson SJ. 2015. The spatial and temporal patterns of erosion rate in the southern Central Range of Taiwan. *AGU Fall Meeting Abstracts* **33**. http://adsabs.harvard.edu/abs/2015AGUFM.T33A2918C [10 January 2017].

Chen C-Y, Willett SD. 2016. Graphical methods of river profile analysis to unravel drainage area change, uplift and erodibility contrasts in the Central Range of Taiwan. *Earth Surface Processes and Landforms* **41**: 2223–2238. https://doi.org/10.1002/esp.3986.

Chen H, Petley DN. 2005. The impact of landslides and debris flows triggered by Typhoon Mindulle in Taiwan. *Quarterly Journal of Engineering Geology and Hydrogeology* **38**: 301–304. https://doi.org/10.1144/1470-9236/04-077.

Chien F-C, Kuo H-C. 2011. On the extreme rainfall of Typhoon Morakot (2009). *Journal of Geophysical Research: Atmospheres*, **116**: D05104. https://doi.org/10.1029/2010JD015092.

Chu H-J, Pan T-Y, Liou J-J. 2011. Extreme precipitation estimation with Typhoon Morakot using frequency and spatial analysis. *Terrestrial, Atmospheric and Oceanic Sciences* **22**: 549. https://doi.org/10.3319/TAO.2011.05.10.02(TM).

Croissant T, Lague D, Davy P, Davies T, Steer P. 2017a. A precipiton-based approach to model hydro-sedimentary hazards induced by large sediment supplies in alluvial fans. *Earth Surface Processes and Landforms* **42**: 2054–2067. https://doi.org/10.1002/esp.4171.

Croissant T, Lague D, Steer P, Davy P. 2017b. Rapid post-seismic landslide evacuation boosted by dynamic river width. *Nature Geoscience* **10**: 680. https://doi.org/10.1038/ngeo3005.

Cui Y, Parker G. 2005. Numerical model of sediment pulses and sediment-supply disturbances in mountain rivers. *Journal of Hydraulic Engineering* **131**: 646. https://doi.org/10.1061/(ASCE)0733-9429(2005)131:8(646).

Culling WEH. 1960. Analytical theory of erosion. *The Journal of Geology* **68**: 336–344. https://doi.org/10.1086/626663.

Dadson SJ et al. 2004. Earthquake-triggered increase in sediment delivery from an active mountain belt. *Geology* **32**: 733–736. https://doi.org/10.1130/G20639.1.

Derrieux F, Siame LL, Bourlès DL, Chen R-F, Braucher R, Léanni L, Lee J-C, Chu H-T, Byrne TB. 2014. How fast is the denudation of the Taiwan mountain belt? Perspectives from *in situ* cosmogenic ^{10}Be. *Journal of Asian Earth Sciences* **88**: 230–245. https://doi.org/10.1016/j.jseaes.2014.03.012.

Dingle EH, Attal M, Sinclair HD. 2017. Abrasion-set limits on Himalayan gravel flux. *Nature* **544**: 471–474. https://doi.org/10.1038/nature22039.

Fellin MG, Chen C-Y, Willett SD, Christl M, Chen Y-G. 2017. Erosion rates across space and timescales from a multi-proxy study of rivers of eastern Taiwan. *Global and Planetary Change* **157**: 174–193. https://doi.org/10.1016/j.gloplacha.2017.07.012.

Finnegan NJ, Roe G, Montgomery DR, Hallet B. 2005. Controls on the channel width of rivers: Implications for modeling fluvial incision of bedrock. *Geology* **33**: 229–232. https://doi.org/10.1130/G21171.1.

Finnegan NJ, Sklar LS, Fuller TK. 2007. Interplay of sediment supply, river incision, and channel morphology revealed by the transient evolution of an experimental bedrock channel. *Journal of Geophysical Research: Earth Surface* **112** F03S11. DOI: https://doi.org/10.1029/2006JF000569.

Fisher GB, Bookhagen B, Amos CB. 2013. Channel planform geometry and slopes from freely available high-spatial resolution imagery and DEM fusion: implications for channel width scalings, erosion proxies, and fluvial signatures in tectonically active landscapes. *Geomorphology* **194**: 46–56. https://doi.org/10.1016/j.geomorph.2013.04.011.

Flint JJ. 1974. Stream gradient as a function of order, magnitude, and discharge. *Water Resources Research* **10**: 969–973. https://doi.org/10.1029/WR010i005p00969.

Fuller CW, Willett SD, Fisher D, Lu CY. 2006. A thermomechanical wedge model of Taiwan constrained by fission-track thermochronometry. *Tectonophysics* **425**: 1–24. https://doi.org/10.1016/j.tecto.2006.05.018.

Gasparini NM, Whipple KX. 2014. Diagnosing climatic and tectonic controls on topography: eastern flank of the northern Bolivian Andes. *Lithosphere* **6**: 230–250. https://doi.org/10.1130/L322.1.

Ge X, Li T, Zhang S, Peng M. 2010. What causes the extremely heavy rainfall in Taiwan during Typhoon Morakot (2009)? *Atmospheric Science Letters* **11**: 46–50. https://doi.org/10.1002/asl.255.

Goode JR, Wohl E. 2010. Substrate controls on the longitudinal profile of bedrock channels: Implications for reach-scale roughness. *Journal of Geophysical Research: Earth Surface* **115**: F03018. https://doi.org/10.1029/2008JF001188.

Goswami DC. 1985. Brahmaputra River, Assam, India: physiography, basin denudation, and channel aggradation. *Water Resources Research* **21**: 959–978. https://doi.org/10.1029/WR021i007p00959.

Hall JD, Xue M, Ran L, Leslie LM. 2012. High-resolution modeling of Typhoon Morakot (2009): vortex Rossby waves and their role in extreme precipitation over Taiwan. *Journal of the Atmospheric Sciences* **70**: 163–186. https://doi.org/10.1175/JAS-D-11-0338.1.

Hendricks EA, Jin Y, Moskaitis JR, Doyle JD, Peng MS, Wu C-C, Kuo H-C. 2015. Numerical simulations of Typhoon Morakot (2009) using a multiply nested tropical cyclone prediction model. *Weather and Forecasting* **31**: 627–645. https://doi.org/10.1175/WAF-D-15-0016.1.

Hong C-C, Lee M-Y, Hsu H-H, Kuo J-L. 2010. Role of submonthly disturbance and 40–50 day ISO on the extreme rainfall event associated with Typhoon Morakot (2009) in southern Taiwan. *Geophysical Research Letters* **37**: L08805. https://doi.org/10.1029/2010GL042761.

Hovius N, Meunier P, Lin C-W, Chen H, Chen Y-G, Dadson S, Horng M-J, Lines M. 2011. Prolonged seismically induced erosion and the mass balance of a large earthquake. *Earth and Planetary Science Letters* **304**: 347–355. https://doi.org/10.1016/j.epsl.2011.02.005.

Hsu H-L, Yanites BJ, Chen C, Chen Y-G. 2010. Bedrock detection using 2D electrical resistivity imaging along the Peikang River, central Taiwan. *Geomorphology* **114**: 406–414. https://doi.org/10.1016/j.geomorph.2009.08.004.

Hsu W-H, Byrne TB, Ouimet W, Lee Y-H, Chen Y-G, van Soest M, Hodges K. 2016. Pleistocene onset of rapid, punctuated exhumation in the eastern Central Range of the Taiwan orogenic belt. *Geology* **44**: 719–722. https://doi.org/10.1130/G37914.1.

Huang J-C, Milliman JD, Lee T-Y, Chen Y-C, Lee J-F, Liu C-C, Lin J-C, Kao S-J. 2017. Terrain attributes of earthquake- and rainstorm-induced landslides in orogenic mountain belt, Taiwan. *Earth Surface Processes and Landforms* **42**(10): 1549–1559. https://doi.org/10.1002/esp.4112.

Hung J-J. 2000. Chi-Chi earthquake induced landslides in Taiwan. *Earthquake Engineering and Engineering Seismology* **2**: 25–33.

Johnson JPL, Whipple KX, Sklar LS, Hanks TC. 2009. Transport slopes, sediment cover, and bedrock channel incision in the Henry Mountains, Utah. *Journal of Geophysical Research: Earth Surface* **114**: F02014. https://doi.org/10.1029/2007JF000862.

Kargel JS et al. 2016. Geomorphic and geologic controls of geohazards induced by Nepal's 2015 Gorkha earthquake. *Science* **351** aac8353. DOI: https://doi.org/10.1126/science.aac8353.

Lague D. 2010. Reduction of long-term bedrock incision efficiency by short-term alluvial cover intermittency. *Journal of Geophysical Research* **115** F02011. DOI: 2010https://doi.org/10.1029/2008JF001210.

Lane SN, Tayefi V, Reid SC, Yu D, Hardy RJ. 2007. Interactions between sediment delivery, channel change, climate change and flood risk in a temperate upland environment. *Earth Surface Processes and Landforms* **32**: 429–446. https://doi.org/10.1002/esp.1404.

Larsen IJ, Montgomery DR. 2012. Landslide erosion coupled to tectonics and river incision. *Nature Geoscience* **5**: 468–473. https://doi.org/10.1038/ngeo1479.

Li G, West AJ, Densmore AL, Hammond DE, Jin Z, Zhang F, Wang J, Hilton RG. 2016. Connectivity of earthquake-triggered landslides with the fluvial network: implications for landslide sediment transport after the 2008 Wenchuan earthquake: Wenchuan landslide distribution. *Journal of Geophysical Research: Earth Surface* **121**: 703–724. https://doi.org/10.1002/2015JF003718.

Lin C-W, Chang W-S, Liu S-H, Tsai T-T, Lee S-P, Tsang Y-C, Shieh C-L, Tseng C-M. 2011. Landslides triggered by the 7 August 2009 Typhoon Morakot in southern Taiwan. *Engineering Geology* **123**: 3–12. https://doi.org/10.1016/j.enggeo.2011.06.007.

Lisle TE. 1982. Effects of aggradation and degradation on riffle-pool morphology in natural gravel channels, northwestern California. *Water Resources Research* **18**: 1643–1651. https://doi.org/10.1029/WR018i006p01643.

McPhillips D, Bierman PR, Rood DH. 2014. Millennial-scale record of landslides in the Andes consistent with earthquake trigger. *Nature Geoscience* **7**: 925–930. https://doi.org/10.1038/ngeo2278.

Montgomery DR. 2001. Slope distributions, threshold hillslopes, and steady-state topography. *American Journal of Science* **301**: 432–454. https://doi.org/10.2475/ajs.301.4-5.432.

Montgomery DR, Brandon MT. 2002. Topographic controls on erosion rates in tectonically active mountain ranges. *Earth and Planetary Science Letters* **201**: 481–489. https://doi.org/10.1016/S0012-821X(02)00725-2.

Montgomery DR, Foufoula-Georgiou E. 1993. Channel network source representation using digital elevation models. *Water Resources Research* **29**: 3925–3934. https://doi.org/10.1029/93WR02463.

Montgomery DR, Gran KB. 2001. Downstream variations in the width of bedrock channels. *Water Resources Research* **37**: 1841–1846. https://doi.org/10.1029/2000WR900393.

Montgomery DR, Huang MY-F, Huang AY-L. 2014. Regional soil erosion in response to land use and increased typhoon frequency and intensity, Taiwan. *Quaternary Research* **81**: 15–20. https://doi.org/10.1016/j.yqres.2013.10.005.

Mukherjee S, Joshi PK, Mukherjee S, Ghosh A, Garg RD, Mukhopadhyay A. 2013. Evaluation of vertical accuracy of open source digital elevation model (DEM). *International Journal of Applied Earth Observation and Geoinformation* **21**: 205–217. https://doi.org/10.1016/j.jag.2012.09.004.

Nelson PA, Seminara G. 2011. Modeling the evolution of bedrock channel shape with erosion from saltating bed load. *Geophysical Research Letters* **38** L17406. DOI: 2011https://doi.org/10.1029/2011GL048628.

Nguyen HT, Wiatr T, Fernández-Steeger TM, Reicherter K, Rodrigues DMM, Azzam R. 2013. Landslide hazard and cascading effects following the extreme rainfall event on Madeira Island (February 2010). *Natural Hazards* **65**: 635–652. https://doi.org/10.1007/s11069-012-0387-y.

Parker RN, Densmore AL, Rosser NJ, de Michele M, Li Y, Huang R, Whadcoat S, Petley DN. 2011. Mass wasting triggered by the 2008 Wenchuan earthquake is greater than orogenic growth. *Nature Geoscience* **4**: 449–452. https://doi.org/10.1038/ngeo1154.

Pearce AJ, Watson AJ. 1986. Effects of earthquake-induced landslides on sediment budget and transport over a 50-yr period. *Geology* **14**: 52–55. https://doi.org/10.1130/0091-7613(1986)14%3C52:EOELOS%3E2.0.CO;2.

Perron JT, Royden L. 2013. An integral approach to bedrock river profile analysis. *Earth Surface Processes and Landforms* **38**: 570–576. https://doi.org/10.1002/esp.3302.

Poddar M. 1952. *Preliminary Report of the Assam Earthquake, 15th August, 1950*. Central Book Department: London.

Rathburn SL, Bennett GL, Wohl EE, Briles C, McElroy B, Sutfin N. 2017. The fate of sediment, wood, and organic carbon eroded during an extreme flood, Colorado Front Range, USA. *Geology* **45**(6): 499–502. https://doi.org/10.1130/G38935.

Riebe CS, Kirchner JW, Granger DE, Finkel RC. 2000. Erosional equilibrium and disequilibrium in the Sierra Nevada, inferred from cosmogenic ^{26}Al and ^{10}Be in alluvial sediment. *Geology* **28**: 803–806. https://doi.org/10.1130/0091-7613(2000)28%3C803:EEADIT%3E2.0.CO;2.

Roback K, Clark MK, West AJ, Zekkos D, Li G, Gallen SF, Chamlagain D, Godt JW. 2018. The size, distribution, and mobility of landslides caused by the 2015 Mw7.8 Gorkha earthquake, Nepal. *Geomorphology* **301**: 121–138. https://doi.org/10.1016/j.geomorph.2017.01.030.

Robinson TR, Davies TRH. 2013. Review Article: Potential geomorphic consequences of a future great (Mw = 8.0+) Alpine Fault earthquake, South Island, New Zealand. *Natural Hazards and Earth System Science* **13**: 2279–2299. https://doi.org/10.5194/nhess-13-2279-2013.

Roering JJ, Kirchner JW, Dietrich WE. 2001. Hillslope evolution by nonlinear, slope-dependent transport: steady state morphology and equilibrium adjustment timescales. *Journal of Geophysical Research: Solid Earth* **106**: 16499–16513. https://doi.org/10.1029/2001JB000323.

Schmidt KM, Montgomery DR. 1995. Limits to relief. *Science* **270**: 617–620. https://doi.org/10.1126/science.270.5236.617.

Schwanghart W et al. 2016. Repeated catastrophic valley infill following medieval earthquakes in the Nepal Himalaya. *Science* **351**: 147–150. https://doi.org/10.1126/science.aac9865.

Schwanghart W, Kuhn NJ. 2010. TopoToolbox: a set of Matlab functions for topographic analysis. *Environmental Modelling & Software* **25**: 770–781. https://doi.org/10.1016/j.envsoft.2009.12.002.

Schwanghart W, Scherler D. 2014. Short Communication: TopoToolbox 2 – MATLAB-based software for topographic analysis and modeling in Earth surface sciences. *Earth Surface Dynamics* **2**: 1–7. https://doi.org/10.5194/esurf-2-1-2014.

Sklar LS, Dietrich WE. 2006. The role of sediment in controlling steady-state bedrock channel slope: implications of the saltation–abrasion incision model. *Geomorphology* **82**: 58–83. https://doi.org/10.1016/j.geomorph.2005.08.019.

Snyder NP, Whipple KX, Tucker GE, Merritts DJ. 2000. Landscape response to tectonic forcing: digital elevation model analysis of stream profiles in the Mendocino triple junction region, northern California. *Geological Society of America Bulletin* **112**: 1250–1263. https://doi.org/10.1130/0016-7606(2000)112%3C1250:LRTTFD%3E2.0.CO;2.

Spotila JA, Moskey KA, Prince PS. 2015. Geologic controls on bedrock channel width in large, slowly-eroding catchments: case study of the New River in eastern North America. *Geomorphology* **230**: 51–63. https://doi.org/10.1016/j.geomorph.2014.11.004.

Stark CP, Barbour JR, Hayakawa YS, Hattanji T, Hovius N, Chen H, Lin C-W, Horng M-J, Xu K-Q, Fukahata Y. 2010. The climatic signature of incised river meanders. *Science* **327**: 1497–1501. https://doi.org/10.1126/science.1184406.

Stover SC, Montgomery DR. 2001. Channel change and flooding, Skokomish River, Washington. *Journal of Hydrology* **243**: 272–286. https://doi.org/10.1016/S0022-1694(00)00421-2.

Suppe J. 1984. *Kinematics of Arc-continent Collision, Flipping of Subduction, and Back-arc Spreading near Taiwan*. Beijing: Memoir of the Geological Society of China; 21.

Tachikawa T, Hato M, Kaku M, Iwasaki A. 2011. Characteristics of ASTER GDEM version 2. *Presented at the 2011 IEEE International Geoscience and Remote Sensing Symposium*, July; 3657–3660.

Tsou C-Y, Feng Z-Y, Chigira M. 2011. Catastrophic landslide induced by Typhoon Morakot, Shiaolin, Taiwan. *Geomorphology* **127**: 166–178. https://doi.org/10.1016/j.geomorph.2010.12.013.

Turowski JM, Lague D, Hovius N. 2007. Cover effect in bedrock abrasion: a new derivation and its implications for the modeling of bedrock channel morphology. *Journal of Geophysical Research: Earth Surface* **112**: F04006. https://doi.org/10.1029/2006JF000697.

Turowski JM, Lague D, Hovius N. 2009. Response of bedrock channel width to tectonic forcing: Insights from a numerical model, theoretical considerations, and comparison with field data. *Journal of Geophysical Research* **114**: F03016. https://doi.org/10.1029/2008JF001133.

Wang J, Jin Z, Hilton RG, Zhang F, Densmore AL, Li G, West AJ. 2015. Controls on fluvial evacuation of sediment from earthquake-triggered landslides. *Geology* **43**: 115–118. https://doi.org/10.1130/G36157.1.

West AJ, Lin C-W, Lin T-C, Hilton RG, Liu S-H, Chang C-T, Lin K-C, Galy A, Sparkes RB, Hovius N. 2011. Mobilization and transport of coarse woody debris to the oceans triggered by an extreme tropical storm. *Limnology and Oceanography* **56**: 77–85. https://doi.org/10.4319/lo.2011.56.1.0077.

Whipple KX, Hancock GS, Anderson RS. 2000. River incision into bedrock: mechanics and relative efficacy of plucking, abrasion, and cavitation. *Geological Society of America Bulletin* **112**: 490–503. https://doi.org/10.1130/0016-7606(2000)112%3C490:RIIBMA%3E2.0.CO;2.

Whipple KX, Tucker GE. 1999. Dynamics of the stream-power river incision model: Implications for height limits of mountain ranges, landscape response timescales, and research needs. *Journal of Geophysical Research* **104**: 17661–17674. DOI: 1999https://doi.org/10.1029/1999JB900120

Whittaker AC, Cowie PA, Attal M, Tucker GE, Roberts GP. 2007. Bedrock channel adjustment to tectonic forcing: Implications for predicting river incision rates. *Geology* **35**: 103–106. https://doi.org/10.1130/G23106A.1.

Wickert AD, Martin JM, Tal M, Kim W, Sheets B, Paola C. 2013. River channel lateral mobility: metrics, time scales, and controls. *Journal of Geophysical Research: Earth Surface* **118**: 396–412. https://doi.org/10.1029/2012JF002386.

Wiltschko DV, Hassler L, Hung J-H, Liao H-S. 2010. From accretion to collision: motion and evolution of the Chaochou Fault, southern Taiwan. *Tectonics* **29**: TC2015. https://doi.org/10.1029/2008TC002398.

Wobus C, Whipple KX, Kirby E, Snyder N, Johnson J, Spyropolou K, Crosby B, Sheehan D. 2006a. Tectonics from topography: Procedures, promise, and pitfalls. *Geological Society of America Special Papers* **398**: 55–74. https://doi.org/10.1130/2006.2398(04).

Wobus CW, Tucker GE, Anderson RS. 2006b. Self-formed bedrock channels. *Geophysical Research Letters* **33**: L18408. https://doi.org/10.1029/2006GL027182.

Wohl E, David GCL. 2008. Consistency of scaling relations among bedrock and alluvial channels. *Journal of Geophysical Research* **113**: F04013. https://doi.org/10.1029/2008JF000989.

Wolman, Miller JP. 1960. Magnitude and frequency of forces in geomorphic processes. *The Journal of Geology* **68**: 54–74.

Wu L, Liang J, Wu C-C. 2011. Monsoonal influence on Typhoon Morakot (2009). Part I: observational analysis. *Journal of the Atmospheric Sciences* **68**: 2208–2221. https://doi.org/10.1175/2011JAS3730.1.

Xu X, Lu C, Xu H, Chen L. 2011. A possible mechanism responsible for exceptional rainfall over Taiwan from Typhoon Morakot. *Atmospheric Science Letters* **12**: 294–299. https://doi.org/10.1002/asl.338.

Yanites BJ, Tucker GE. 2010. Controls and limits on bedrock channel geometry. *Journal of Geophysical Research* **115**: F04019. DOI: 2010https://doi.org/10.1029/2009JF001601

Yanites BJ, Tucker GE, Hsu H-L, Chen C, Chen Y-G, Mueller KJ. 2011. The influence of sediment cover variability on long-term river incision rates: an example from the Peikang River, central Taiwan. *Journal of Geophysical Research: Earth Surface* **116**: F03016. https://doi.org/10.1029/2010JF001933.

Yanites BJ, Tucker GE, Mueller KJ, Chen Y-G. 2010a. How rivers react to large earthquakes: evidence from central Taiwan. *Geology* **38**: 639–642. https://doi.org/10.1130/G30883.1.

Yanites BJ, Tucker GE, Mueller KJ, Chen Y-G, Wilcox T, Huang S-Y, Shi K-W. 2010b. Incision and channel morphology across active structures along the Peikang River, central Taiwan: implications for the importance of channel width. *Geological Society of America Bulletin* **122**: 1192–1208. https://doi.org/10.1130/B30035.1.

Yen T-H, Wu C-C, Lien G-Y. 2011. Rainfall simulations of Typhoon Morakot with controlled translation speed based on EnKF data assimilation. *Terrestrial, Atmospheric and Oceanic Sciences* **22**: 647–660.

Zhang F, Weng Y, Kuo Y-H, Whitaker JS, Xie B. 2010. Predicting Typhoon Morakot's catastrophic rainfall with a convection-permitting mesoscale ensemble system. *Weather and Forecasting* **25**: 1816–1825. https://doi.org/10.1175/2010WAF2222414.1.